

Multi-microjoule GaSe-based mid-infrared optical parametric amplifier with an ultra-broad idler spectrum covering 4.2-16 μm

KUN LIU^{1,2}, HOUKUN LIANG^{1,*}, LIFENG WANG¹, SHIZHEN QU^{1,2}, TINO LANG³, HAO LI¹, QI JIE WANG^{2,*}, YING ZHANG¹

¹ Precision Measurements Group, Singapore Institute of Manufacturing Technology, 2 Fusionopolis Way, 138634, Singapore

² School of Electrical & Electronic Engineering & The Photonics Institute, Nanyang Technological University 639798, Singapore

³ Center for Free-Electron Laser Science, DESY, Notkestraße 85, 22607 Hamburg, Germany

*Corresponding author: hkliang@simtech.a-star.edu.sg, qjwang@ntu.edu.sg

Received XX Month XXXX; revised XX Month, XXXX; accepted XX Month XXXX; posted XX Month XXXX (Doc. ID XXXXX); published XX Month XXXX

We report a multi-microjoule, ultra-broadband mid-infrared optical parametric amplifier based on a GaSe nonlinear crystal pumped at $\sim 2 \mu\text{m}$. The generated idler pulse has a flat spectrum spanning from 4.5 to 13.3 μm at -3 dB and 4.2 to 16 μm in the full spectral range, with a central wavelength of 8.8 μm . The proposed scheme supports a sub-cycle Fourier-transform-limited pulse width. A (2+1)-dimensional numerical simulation is employed to reproduce the obtained idler spectrum. To our best knowledge, this is the broadest -3 dB spectrum ever obtained by optical parametric amplifiers in this spectral region. The idler pulse energy is $\sim 3.4 \mu\text{J}$ with a conversion efficiency of $\sim 2\%$ from the $\sim 2 \mu\text{m}$ pump to the idler pulse.

OCIS codes: (140.3070) Infrared and far-infrared lasers; (190.4360) Nonlinear optics, devices; (190.4410) Nonlinear optics, parametric processes; (190.7110) ultrafast nonlinear optics.

<http://dx.doi.org/10.1364/OL.99.099999>

High-energy ultra-broadband few-cycle mid-infrared (mid-IR) sources have attracted extensive attention for their applications in molecular spectroscopy [1-4] and strong-field physics [5-14]. In recent years, the development of such sources has been extended to $>6 \mu\text{m}$ long-wavelength region. In the perspective of molecular spectroscopy, the long-wavelength mid-IR is more suitable for identification of molecules, because the vibrational absorption spectrum of each molecule in the wavelength range of 6.7-25 μm , i.e. the fingerprint region, is distinctive [3, 4]. In strong-field physics, energy of the re-colliding electrons increases substantially with the driving wavelength, which enables the tunneling ionization even at moderate laser intensity, without causing an optical damage. This has triggered a number of studies on ultrafast electronics in

molecules, solid materials as well as nano-structures [7-14]. In addition, long-wavelength mid-IR pulses have their photon energies far below the typical electronic interband resonances of bulk semiconductors. Therefore, phase-stable few-cycle long-wavelength mid-IR pulses could serve as a precisely adjustable bias for studies of ultrafast electronics [11]. With the demand for high-fidelity mid-IR spectroscopy and strong-field electron dynamics, high-energy few-cycle long-wavelength mid-IR lasers with stable carrier-envelope phase (CEP) are highly desired.

In the absence of broadband laser gain media in the mid-IR region, parametric down conversions such as optical parametric amplifier (OPA), optical parametric chirped-pulse amplifier (OPCPA) and difference-frequency generation (DFG) are commonly used to generate high-energy few-cycle mid-IR pulses. Non-oxide nonlinear crystals such as AgGaS_2 [15, 16], CdSiP_2 [17], and ZnGeP_2 [18-20] are employed to extend high-energy few-cycle pulses to the wavelength range of 4-11 μm . 8.5 μm , 150 μJ , few-cycle pulses are demonstrated by mixing the 1.8 μm pump and the 2.4 μm signal in an AgGaS_2 -based DFG system [15]. 33 μJ , 0.88-cycle pulses covering 2.5-10 μm spectral range are generated by coherent synthesis of signal and idler pulses of a CdSiP_2 OPA, pumped by a 2 μm OPCPA [17]. The energy of a few-cycle ZnGeP_2 -based OPCPA system at a central wavelength of 7 μm is boosted to half millijoule, with a powerful 2 μm cryogenic-cooled pump [18]. Recently, the wide bandgap nonlinear crystal LiGaS_2 has emerged. 7-11 μm few-cycle pulses with nano-joule-level pulse energy have been demonstrated in OPA and/or intrapulse DFG configurations based on LiGaS_2 crystal and pumped at the near-IR [21-24]. To pursue longer wavelength up to 20 μm , AgGaSe_2 [25, 26] and GaSe [27-29] nonlinear crystals have been employed in the DFG configuration, thanks to their longer transparent cutoff wavelength. In order to achieve broad phase-matching (PM) bandwidth and avoid parasitic two- or three-photon absorption, such light sources should ideally be pumped at $\sim 2 \mu\text{m}$ wavelength [29]. Compared to AgGaSe_2 , GaSe has higher damage threshold, larger nonlinear coefficient, larger

birefringence (shown in Table. 1) and broader PM bandwidth pumped at $\sim 2 \mu\text{m}$ wavelength [25-29]. These make GaSe a better candidate for generation of high-energy ultra-broadband few-cycle long-wavelength mid-IR pulses.

Table. 1 A comparison between GaSe and AgGaSe₂. Nonlinear coefficients (d_{eff}) are taken from SNLO for $8 \mu\text{m}$ idler.

| Crystals | Type-I,II d_{eff} (pm/V) | Birefringence (Δn) | Damage threshold (TW/cm ²) | Transmission (μm) |
|---------------------|-----------------------------------|------------------------------|--|--------------------------------|
| GaSe | 57,55 | 0.34 [30] | 1.7 [28] | 0.65-18 [30] |
| AgGaSe ₂ | 25,33 | -0.024 [30] | >0.2 [25] | 0.78-18 [30] |

In this letter, we report a GaSe-based mid-IR OPA driven by a $\sim 2 \mu\text{m}$ source. The generated ultra-broadband idler pulse has a spectrum spanning from 4.2 to 16 μm , which supports a Fourier-transform-limited pulse width of ~ 19 fs (0.65 cycle), centered at 8.8 μm . The spectrum is much broader than the reported parametric sources based on other nonlinear crystals [15-26]. $\sim 3.4 \mu\text{J}$ idler pulse energy is obtained with a conversion efficiency of $\sim 2\%$. We believe the generated multi-microjoule, few-cycle, ultra-broadband, long-wavelength mid-IR pulses would be impactful for both mid-IR molecular spectroscopy and ultrafast electron dynamics studies.

Type-I phase match is used in GaSe due to its broader PM bandwidth compared with Type-II phase match [29]. Fig. 1 shows the PM function $|\text{sinc}(\Delta kL/2)|$ with respect to the PM angle and the PM wavelength, where a 1-mm thick GaSe crystal and a pump wavelength of $2.15 \mu\text{m}$ are used for the calculation. Within 0.4 degree deviation of the PM angle, centered at $\sim 11.1^\circ$, the PM bandwidth of the idler pulse ranging from 4 to 16 μm could be realized. It is worth mentioning that when a broadband pump source is used, even broader PM bandwidth can be obtained.

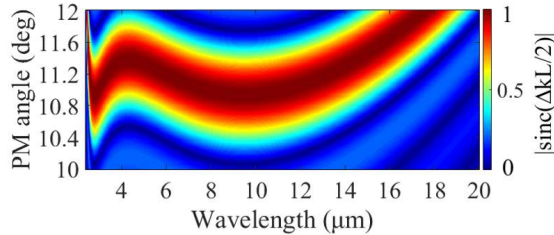


Fig. 1. The phase-matching (PM) function $|\text{sinc}(\Delta kL/2)|$ with respect to the PM angle and the PM wavelength, in a GaSe crystal with a length (L) of 1 mm, for the Type-I phase match, at a $2.15 \mu\text{m}$ pump wavelength.

The schematic of the mid-IR OPA is shown in Fig. 2(a). The pump source is a commercial multi-stage OPA system (TOPAS from Light Conversion, which is driven by a 5 mJ, 26 fs, 800 nm Ti: Sapphire laser system) with a $2.15 \mu\text{m}$ central wavelength, 420 μJ pulse energy, 51 fs pulse width, and 1 kHz repetition rate. A CaF_2 wedge placed at 22° with respect to the pump beam, functioning as a beam splitter, is employed to reflect $\sim 10 \mu\text{J}$, $2.15 \mu\text{m}$, p -polarized pump for the supercontinuum (SC) generation. It is rotated to s -polarization by a half-wave plate, and focused into a 6-mm thick BaF_2 by L_1 to generate signal pulses via SC. The generated SC is collimated by L_2 and resized to $\sim 2.5 \text{ mm } 1/e^2$ diameter by a telescope comprised of L_3 and L_4 . The transmitted $2.15 \mu\text{m}$ enters the pump line, which includes a delay line and a telescope (L_5 and

L_6), to form a collimated pump beam with a comparable beam size as that of the signal beam.

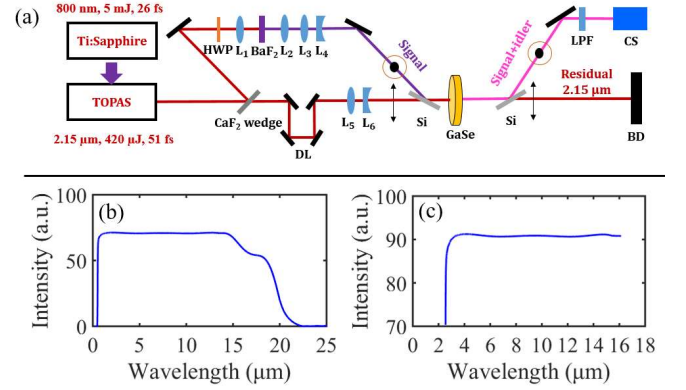


Fig. 2. (a) The schematic of the GaSe-based mid-IR optical parametric amplifier (OPA). The pump, the generated supercontinuum, and the amplified mid-IR pulses are shown in maroon, purple, and pink, respectively. (HWP-half wave plate, DL-delay line, LPF-long pass filter, BD-beam dump, CS-characterization setup, and L_1 - L_6 are CaF_2 lenses.) The transmission curves of the uncoated ZnSe lens (b) and the mid-IR hollow-core fiber (c).

The collimated beam is then employed to pump a 1 mm-thick uncoated GaSe crystal with a Type-I phase match. As the GaSe crystal could be cleaved only along the (001) plane (z -cut, $\theta = 0^\circ$), an internal PM angle of $\sim 11.1^\circ$ corresponding to an external angle of $\sim 32^\circ$ is introduced. This causes $\sim 16\%$ loss for the p -polarized pump. It is noted that the pump beam is routed to the crystal using multiple silver mirrors with a $\sim 96\%$ reflection for each. Taking into account all the losses, the maximum available pulse energy of the $2.15 \mu\text{m}$ pump is $\sim 300 \mu\text{J}$, giving an estimated peak intensity of $\sim 224 \text{ GW/cm}^2$. Two 200- μm thick silicon windows placed at a Brewster angle of 73.8° with respect to the pump beam are used as the beam combiner and beam splitter, respectively. This produces $\sim 71\%$ reflection for the s -polarized signal and idler beams. The generated idler beam is separated from the amplified signal beam using a long-pass filter (LPF) with a cut-off wavelength of $4.5 \mu\text{m}$. A thermal sensitive power meter with a resolution of $1 \mu\text{W}$ (S401C, Thorlabs) and a calibrated mid-IR monochromator with a liquid-nitrogen-cooled HgCdTe (MCT) detector are used to characterize the mid-IR pulses. For the spectral measurement, an uncoated ZnSe lens with a near-flat transmission over 1-15 μm (Fig. 2(b)) and a dielectric-coated mid-IR hollow-core fiber with a 500- μm core diameter (HF500MW, OptoKnowledge) are employed to couple the mid-IR pulses into the monochromator. The hollow-core fiber has a near-flat transmission in the range of 3-16 μm (Fig. 2(c)).

The spectral and temporal profiles of the $2.15 \mu\text{m}$ pump from TOPAS are firstly characterized. The measured spectrum as shown in Fig. 3(a) has a full width at half maximum of $\sim 220 \text{ nm}$ which supports ~ 31 fs Fourier-transform-limited pulse width. The intensity autocorrelation shown in Fig. 3(b) reveals the pulse width of ~ 51 fs, assuming a Gaussian temporal profile. This agrees with the residual dispersion from the TOPAS optics, including about -400 fs^2 dispersion from the 3 mm fused silica beam splitter (reflecting 800 nm, and transmitting $2.15 \mu\text{m}$). Fig. 3(c) shows the long-wavelength side of the SC spectrum (measured through a InF_3 fiber and a $2.4 \mu\text{m}$ LPF) which serves as the signal of the mid-IR OPA. It extends up to $\sim 4.3 \mu\text{m}$. With the knowledge of the long-

wavelength edge of the signal, the calculated spectral edge on the short-wavelength side of the generated idler is $<4.3 \mu\text{m}$, which means the signal and idler overlap in the frequency domain. Thus a LPF with a $4.5 \mu\text{m}$ cut-off wavelength is employed to separate the generated idler from the amplified signal.

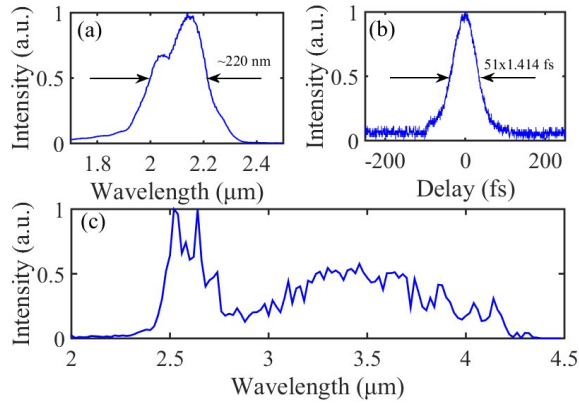


Fig. 3. (a) The measured pump spectrum from the TOPAS source with a $\sim 420 \mu\text{J}$ output energy. (b) The intensity autocorrelation trace of the pump pulses with the $\sim 420 \mu\text{J}$ output energy. (c) The supercontinuum generated from 6-mm-thick BaF_2 , which serves as the signal of the mid-IR OPA, measured using $2.4 \mu\text{m}$ LPF and InF_3 fiber with $300\text{-}\mu\text{m}$ core diameter.

An ultra-broadband idler spectrum is obtained by carefully optimizing the crystal angle, temporal and spatial overlaps between the pump and the signal. The idler spectrum spans from 4.2 to $16 \mu\text{m}$, with the -3 dB bandwidth ranging from 4.5 to $13.3 \mu\text{m}$, shown in Fig. 4(a). It should be noted that the $4.5 \mu\text{m}$ LPF is responsible for the steep edge at $\sim 4.6 \mu\text{m}$. The distance from the OPA output to the detector of the monochromator is $\sim 3 \text{ m}$, thus some fine structures caused by the atmospheric absorption appear in the spectrum. Similar absorption structures have been reported in the broadband mid-IR systems [18, 31]. In addition, the SC components in the range of $2.5\text{-}3 \mu\text{m}$ are located in the water absorption window. These absorption structures are transferred to the $7\text{-}15 \mu\text{m}$ idler spectrum during the parametric amplification, which also contributes to the fine structures of the idler spectrum. A vacuum or noble gas purging chamber could be used to remove these spectral structures [28].

The OPA process is further investigated using a (2+1)-dimensional numerical simulation [32]. Taking into account the high pump intensity and the large nonlinear refractive index of GaSe ($n_2 = 450 \times 10^{-1} \text{ cm}^2/\text{W}$) [33], the self-phase modulation and self-focusing are included in the calculations, which are found crucial for reproducing the measured spectrum. A $2.15 \mu\text{m}$, $300 \mu\text{J}$, 50 fs chirped Gaussian pump pulse with a spectrum spanning from 1.8 to $2.3 \mu\text{m}$, and a $2.84 \mu\text{m}$, 3 nJ , 50 fs chirped signal with a spectral shape similar to the measured SC covering 2.3 to $4.3 \mu\text{m}$ are employed in the simulation to mimic the experimental conditions. The PM angle is set to 11.15° . The simulated spectra are shown in Fig. 4(a) and (b), which qualitatively match with the measured idler and amplified signal spectra. The slight mismatch for idler spectrum at $> 13 \mu\text{m}$ is due to the crystal absorption [34].

In order to further verify the accuracy of the measured idler spectrum, we integrate the measured spectrum and calculate the energy distribution in different spectral bands, i.e. $4.2\text{-}7.3 \mu\text{m}$, $7.3\text{-}11.7$

$11.7 \mu\text{m}$, and $11.7\text{-}16 \mu\text{m}$, based on the measured idler pulse energy. We compare the integrated pulse energies with the measured, as shown in Fig. 4(c). The good agreement between the integrated and measured pulse energy gives a direct evidence for the accuracy of the spectrum measurement.

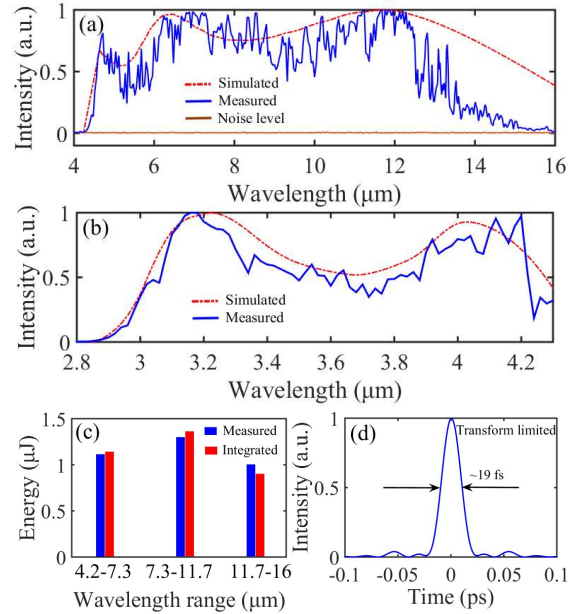


Fig. 4. The measured (solid blue, 20 nm resolution) and simulated (dashed red) spectra of the idler pulses (a) and the amplified signal pulses (b). Note that the measured spectra are calibrated by taking account of the response curves of the grating, MCT, LPF and the hollow-core fiber. The simulated spectra include the edge responses of the hollow-core fiber and LPF. (c) The measured and integrated energy distribution in different bands of the idler wavelength. (d) The calculated Fourier-limited pulse width based on the measured idler spectrum.

Based on the idler spectrum, the calculated transform-limited pulse width is $\sim 19 \text{ fs}$ (Fig. 4(d)), which corresponds to 0.65-cycle pulse width, centered at $8.8 \mu\text{m}$. The actual pulse width could be broadened to few cycles due to the dispersion from the 1 mm thick $4.5 \mu\text{m}$ LPF (Ge substrate) and the intrinsic dispersion from the OPA. It is worth noting that as the signal and the pump are from the same TOPAS pump system, the CEP fluctuation in the idler pulse is self-canceled through the DFG nature of the OPA [35, 36]. Recently, stable CEP of the idler pulse from a passively CEP stable mid-IR OPA has been experimentally confirmed [17]. Thus, we, to the large extent, believe that the CEP for this system is stable. Its CEP stability could be degraded by some factors such as the intensity-to-phase noise of the pump, and the temporal jitters between the pump and the signal [35, 36].

The pulse energy of the generated idler is measured as $\sim 3.4 \mu\text{J}$ behind a $4.5 \mu\text{m}$ LPF, with $\sim 300 \mu\text{J}$ pump energy. Considering the 85% transmission of the LPF and $\sim 71\%$ reflection from the silicon beam splitter for the idler pulses, $\sim 2\%$ conversion efficiency from the pump to the idler is achieved. For this OPA system, the measured OPA output by blocking the signal is $\sim 0.12 \mu\text{J}$, and the energy fluctuation of the generated idler pulses is 2.8% rms for a measurement duration of 30 minutes . In addition, the idler pulse energies with different LPFs as a function of the pump energy are

measured, shown in Fig. 5. No saturation occurs at the maximum pump energy, which implies further energy scaling up is possible with higher pump energy. The idler beam profile behind the 4.5 μm LPF are also measured, exhibiting a good Gaussian profile shown in the inset of Fig. 5.

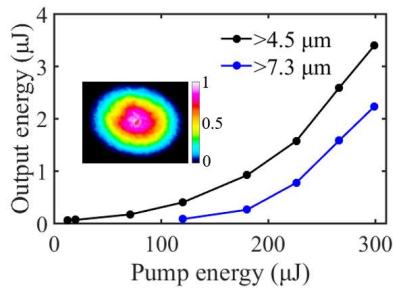


Fig. 5. The dependence of the idler pulse energy on the pump energy behind the 4.5 and 7.3 μm LPFs. The inset is the beam profile of the idler pulse behind the 4.5 μm LPF at the output energy of ~ 3.4 μJ .

In conclusions, 3.4 μJ ultra-broadband mid-IR pulses with a spectrum spanning from 4.5 to 13.3 μm at -3 dB and from 4.2 to 16 μm in the full spectral range are generated from a SC seeded GaSe-based OPA system pumped at ~ 2 μm . To the best of our knowledge, this is the broadest -3 dB spectrum ever obtained by OPA systems in this wavelength region. With the rapid progress of ~ 2 μm Ho:YLF or Ho:YAG CPA systems [18-20, 37], the energy scaling up of the ultra-broadband mid-IR pulses is expected through the development of the GaSe-based OPCPA systems.

Acknowledgement. We acknowledge the financial support from SERC (Grant No.1426500050, and 1426500051) from the Agency for Science, Technology and Research (A*STAR), Singapore.

References

1. A. Schliesser, N. Picqué, and T.W. Hänsch, *Nat. Photonics* **6**, 440 (2012).
2. J. Haas, and B. Mizaikoff, *Annu. Rev. Anal. Chem.* **9**, 45 (2016).
3. O. Kara, L. Maidment, T. Gardiner, P. G. Schunemann, and D. T. Reid, *Opt. Express* **25**, 32713 (2017).
4. H. Timmers, A. Kowligy, A. Lind, F. C. Cruz, N. Nader, M. Silfies, G. Ycas, T. K. Allison, P. G. Schunemann, S. B. Papp, and S. A. Diddams, *Optica* **5**, 727 (2018).
5. J. Li, X. Ren, Y. Yin, K. Zhao, A. Chew, Y. Cheng, E. Cunningham, Y. Wang, S. Hu, Y. Wu, M. Chini and Z. Chang, *Nat. Commun.* **8**, 186 (2017).
6. T. Popmintchev, M.-C. Chen, D. Popmintchev, P. Arpin, S. Brown, S. Ališauskas, G. Andriukaitis, T. Balčiunas, O. D. Mücke, A. Pugzlys, A. Baltuška, B. Shim, S. E. Schrauth, A. Gaeta, C. Hernández-García, L. Plaja, A. Becker, A. Jaron-Becker, M. M. Murnane, and H. C. Kapteyn, *Science* **336**, 1287 (2012).
7. B. Wolter, M. G. Pullen, A.-T. Le, M. Baudisch, K. Doblhoff-Dier, A. Senftleben, M. Hemmer, C. D. Schröter, J. Ullrich, T. Pfeifer, R. Moshhammer, S. Gräfe, O. Vendrell, C. D. Lin, and J. Biegert, *Science* **354**, 308 (2016).
8. L. V. Keldysh, *Sov. Phys. JETP* **20**, 1307 (1965).
9. P. Colosimo, G. Doumy, C. I. Blaga, J. Wheeler, C. Hauri, F. Catoire, J. Tate, R. Chirla, A. M. March, G. G. Paulus, H. G. Muller, P. Agostini and L.F. DiMauro, *Nat. Phys.* **4**, 386 (2008).
10. G. Herink, D. R. Solli, M. Gulde, and C. Ropers, *Nature* **483**, 190 (2012).
11. M. Hohenleutner, F. Langer, O. Schubert, M. Knorr, U. Huttner, S. W. Koch, M. Kira, and Rupert Huber, *Nature* **523**, 572 (2015).
12. S. Ghimire, A. D. DiChiara, E. Sistrunk, P. Agostini, L. F. DiMauro, and D. A. Reis, *Nat. Phys.* **7**, 138 (2011).
13. O. Schubert, M. Hohenleutner, F. Langer, B. Urbanek, C. Lange, U. Huttner, D. Golde, T. Meier, M. Kira, S. W. Koch, and R. Huber, *Nat. Photonics* **8**, 119 (2014).
14. T. Rybka, M. Ludwig, M. F. Schmalz, V. Knittel, D. Brida, and A. Leitenstorfer, *Nat. Photonics* **10**, 667 (2016).
15. G. M. Archipovaite, P. Malevich, E. Cormier, T. Lihao, A. Baltuska, and T. Balciunas, *Advanced Solid State Lasers* (Optical Society of America, 2017), paper AM4A-4.
16. A. A. Lanin, A. A. Voronin, E. A. Stepanov, A. B. Fedotov, and A. M. Zheltikov, *Opt. Lett.* **40**, 974 (2015).
17. H. Liang, P. Krogen, Z. Wang, H. Park, T. Kroh, K. Zawilski, P. Schunemann, J. Moses, L. F. DiMauro, F. X. Kärtner, and K.-H. Hong, *Nat. Commun.* **8**, 141 (2017).
18. D. Sanchez, M. Hemmer, M. Baudisch, S. L. Cousin, K. Zawilski, P. Schunemann, O. Chalus, C. Simon-Boisson, and J. Biegert, *Optica* **3**, 147 (2016).
19. L. Grafenstern, M. Bock, D. Ueberschaer, K. Zawilski, P. Schunemann, U. Griebner, and T. Elsaesser, *Opt. Lett.* **42**, 3796 (2017).
20. T. Kanai, P. Malevich, S. S. Kangaparambil, K. Ishida, M. Mizui, K. Yamanouchi, H. Hoogland, R. Holzwarth, A. Pugzlys, and A. Baltuska, *Opt. Lett.* **42**, 683 (2017).
21. I. Pupeza, D. Sánchez, J. Zhang, N. Lilienfein, M. Seidel, N. Karpowicz, T. Paasch-Colberg, I. Znakovskaya, M. Pescher, W. Schweinberger, V. Pervak, E. Fill, O. Pronin, Z. Wei, F. Krausz, A. Apolonski, and J. Biegert, *Nat. Photonics* **9**, 721 (2015).
22. B.-H. Chen, T. Nagy, and P. Baum, *Opt. Lett.* **43**, 1742 (2018).
23. M. Seidel, X. Xiao, S. A. Hussain, G. Arisholm, A. Hartung, K. T. Zawilski, P. G. Schunemann, F. Habel, M. Trubetskov, V. Pervak, O. Pronin, and F. Krausz, *Sci. Adv.* **4**, eaaq 1526 (2018).
24. S.B. Penwell, L. Whaley-Mayda, and A. Tokmakoff, *Opt. Lett.* **43**, 1363 (2018).
25. O. Novák, P. R. Krogen, T. Kroh, T. Mocek, F. X. Kärtner, and K.-H. Hong, *Opt. Lett.* **43**, 1335 (2018).
26. M. Beutler, I. Rimke, E. Büttner, P. Farinello, A. Agnesi, V. Badikov, D. Badikov, and V. Petrov, *Opt. Express* **23**, 2730 (2015).
27. M. Knorr, J. Raab, M. Tauer, P. Merkl, D. Peller, E. Wittmann, E. Riedle, C. Lange, and R. Huber, *Opt. Lett.* **42**, 4367 (2017).
28. C. Gaida, M. Gebhardt, T. Heuermann, F. Stutzki, C. Jauregui, J. Antonio-Lopez, A. Schülzgen, R. Amezcua-Correa, A. Tünnermann, I. Pupeza, and J. Limpert, *Light Sci. Appl.* **7**, 94 (2018).
29. J. Zhang, K. F. Mak, N. Nagl, M. Seidel, D. Bauer, D. Sutter, V. Pervak, F. Krausz, and O. Pronin, *Light Sci. Appl.* **7**, 17180 (2018).
30. M. J. Weber. *Handbook of optical materials*. CRC press, 2002.
31. D. Sánchez, M. Hemmer, M. Baudisch, K. Zawilski, P. Schunemann, H. Hoogland, R. Holzwarth, and J. Biegert, *Opt. Lett.* **39**, 6883 (2014).
32. T. Lang, A. Harth, J. Matyschok, T. Binhammer, M. Schultze, and U. Morgner, *Opt. Express* **21**, 949 (2013).
33. K. L. Vodopyanov, *Laser Photonics Rev.* **2**, 11 (2008).
34. Z.-S. Feng, Z.-H. Kang, F.-G. Wu, J.-Y. Gao, Y. Jiang, H.-Z. Zhang, Y. M. Andreev, G. V. Lanski, V. V. Atuchin, and T. A. Gavrilova, *Opt. Express* **16**, 9978 (2008).
35. A. Baltuška, T. Fuji, and T. Kobayashi, *Phys. Rev. Lett.* **88**, 133901 (2002).
36. G. Cerullo, A. Baltuška, O. Mücke, and C. Vozzi, *Laser Photonics Rev.* **5**, 323 (2011).
37. L. von Grafenstern, M. Bock, D. Ueberschaer, U. Griebner, and T. Elsaesser, *Opt. Lett.* **41**, 4668 (2016).

Full references

1. A. Schliesser, N. Picqué, and T.W. Hänsch, "Mid-infrared frequency combs," *Nat. Photonics* **6**, 440 (2012).
2. J. Haas, and B. Mizaikoff, "Advances in mid-infrared spectroscopy for chemical analysis," *Annu. Rev. Anal. Chem.* **9**, 45 (2016).
3. O. Kara, L. Maidment, T. Gardiner, P. G. Schunemann, and D. T. Reid, "Dual-comb spectroscopy in the spectral fingerprint region using OPGaP optical parametric oscillators," *Opt. Express* **25**, 32713 (2017).
4. H. Timmers, A. Kowligy, A. Lind, F. C. Cruz, N. Nader, M. Silfies, G. Ycas, T. K. Allison, P. G. Schunemann, S. B. Papp, and S. A. Diddams, "Molecular fingerprinting with bright, broadband infrared frequency combs," *Optica* **5**, 727 (2018).
5. J. Li, X. Ren, Y. Yin, K. Zhao, A. Chew, Y. Cheng, E. Cunningham, Y. Wang, S. Hu, Y. Wu, M. Chini and Z. Chang, "53-attosecond X-ray pulses reach the carbon K-edge," *Nat. Commun.* **8**, 186 (2017).
6. T. Popmintchev, M.-C. Chen, D. Popmintchev, P. Arpin, S. Brown, S. Ališauskas, G. Andriukaitis, T. Balčiunas, O. D. Mücke, A. Pugzlys, A. Baltuška, B. Shim, S. E. Schrauth, A. Gaeta, C. Hernández-García, L. Plaja, A. Becker, A. Jaron-Becker, M. M. Murnane, and H. C. Kapteyn, "Bright coherent ultrahigh harmonics in the keV x-ray regime from midinfrared femtosecond lasers," *Science* **336**, 1287 (2012).
7. B. Wolter, M. G. Pullen, A.-T. Le, M. Baudisch, K. Doblhoff-Dier, A. Sentfleben, M. Hemmer, C. D. Schröter, J. Ullrich, T. Pfeifer, R. Moshhammer, S. Gräfe, O. Vendrell, C. D. Lin, and J. Biegert, "Ultrafast electron diffraction imaging of bond breaking in di-ionized acetylene," *Science* **354**, 308 (2016).
8. L. V. Keldysh, "Ionization in the field of a strong electromagnetic wave," *Sov. Phys. JETP* **20**, 1307 (1965).
9. P. Colosimo, G. Doumy, C. I. Blaga, J. Wheeler, C. Hauri, F. Catoire, J. Tate, R. Chirla, A. M. March, G. G. Paulus, H. G. Muller, P. Agostini and L.F. DiMauro, "Scaling strong-field interactions towards the classical limit," *Nat. Phys.* **4**, 386 (2008).
10. G. Herink, D. R. Solli, M. Gulde, and C. Ropers, "Field-driven photoemission from nanostructures quenches the quiver motion," *Nature* **483**, 190 (2012).
11. M. Hohenleutner, F. Langer, O. Schubert, M. Knorr, U. Huttner, S. W. Koch, M. Kira, and Rupert Huber, "Real-time observation of interfering crystal electrons in high-harmonic generation," *Nature* **523**, 572 (2015).
12. S. Ghimire, A. D. DiChiara, E. Sistrunk, P. Agostini, L. F. DiMauro, and D. A. Reis, "Observation of high-order harmonic generation in a bulk crystal," *Nat. Phys.* **7**, 138 (2011).
13. O. Schubert, M. Hohenleutner, F. Langer, B. Urbanek, C. Lange, U. Huttner, D. Golde, T. Meier, M. Kira, S. W. Koch, and R. Huber, "Sub-cycle control of terahertz high-harmonic generation by dynamical Bloch oscillations," *Nat. Photonics* **8**, 119 (2014).
14. T. Rybka, M. Ludwig, M. F. Schmalz, V. Knittel, D. Brida, and A. Leitenstorfer, "Sub-cycle optical phase control of nanotunnelling in the single-electron regime," *Nat. Photonics* **10**, 667 (2016).
15. G. M. Archipovaite, P. Malevich, E. Cormier, T. Lihao, A. Baltuska, and T. Balciunas, "Efficient few-cycle mid-IR pulse generation in the 5-11 μm window driven by an Yb amplifier," *Advanced Solid State Lasers (Optical Society of America, 2017)*, paper AM4A-4.
16. A. A. Lanin, A. A. Voronin, E. A. Stepanov, A. B. Fedotov, and A. M. Zheltikov, "Multioctave, 3–18 μm sub-two-cycle supercontinua from self-compressing, self-focusing soliton transients in a solid," *Opt. Lett.* **40**, 974 (2015).
17. H. Liang, P. Krogen, Z. Wang, H. Park, T. Kroh, K. Zawilski, P. Schunemann, J. Moses, L. F. DiMauro, F. X. Kärtner, and K.-H. Hong, "High-energy mid-infrared sub-cycle pulse synthesis from a parametric amplifier," *Nat. Commun.* **8**, 141 (2017).
18. D. Sanchez, M. Hemmer, M. Baudisch, S. L. Cousin, K. Zawilski, P. Schunemann, O. Chalus, C. Simon-Boisson, and J. Biegert, "7 μm , ultrafast, sub-millijoule-level mid-infrared optical parametric chirped pulse amplifier pumped at 2 μm ," *Optica* **3**, 147 (2016).
19. L. Grafenstein, M. Bock, D. Ueberschaer, K. Zawilski, P. Schunemann, U. Griebner, and T. Elsaesser, "5 μm few-cycle pulses with multi-gigawatt peak power at a 1 kHz repetition rate," *Opt. Lett.* **42**, 3796 (2017).
20. T. Kanai, P. Malevich, S. S. Kangaparambil, K. Ishida, M. Mizui, K. Yamanouchi, H. Hoogland, R. Holzwarth, A. Pugzlys, and A. Baltuska, "Parametric amplification of 100 fs mid-infrared pulses in ZnGeP2 driven by a Ho:YAG chirped-pulse amplifier," *Opt. Lett.* **42**, 683(2017).
21. I. Pupeza, D. Sánchez, J. Zhang, N. Lilienfein, M. Seidel, N. Karpowicz, T. Paasch-Colberg, I. Znakovskaya, M. Pescher, W. Schweinberger, V. Pervak, E. Fill, O. Pronin, Z. Wei, F. Krausz, A. Apolonski, and J. Biegert, "High-power sub-two-cycle mid-infrared pulses at 100 MHz repetition rate," *Nat. Photonics* **9**, 721 (2015).
22. B.-H. Chen, T. Nagy, and P. Baum, "Efficient middle-infrared generation in LiGaS2 by simultaneous spectral broadening and difference-frequency generation," *Opt. Lett.* **43**, 1742 (2018).
23. M. Seidel, X. Xiao, S. A. Hussain, G. Arisholm, A. Hartung, K. T. Zawilski, P. G. Schunemann, F. Habel, M. Trubetskov, V. Pervak, O. Pronin, and F. Krausz, "Multi-watt, multi-octave, mid-infrared femtosecond source," *Sci. Adv.* **4**, eaaq 1526 (2018).
24. S.B. Penwell, L. Whaley-Mayda, and A. Tokmakoff, "Single-stage MHz mid-IR OPA using LiGaS2 and a fiber laser pump source," *Opt. Lett.* **43**, 1363 (2018).
25. O. Novák, P. R. Krogen, T. Kroh, T. Mocek, F. X. Kärtner, and K.-H. Hong, "Femtosecond 8.5 μm source based on intrapulse difference-frequency generation of 2.1 μm pulses," *Opt. Lett.* **43**, 1335 (2018).
26. M. Beutler, I. Rimke, E. Büttner, P. Farinello, A. Agnesi, V. Badikov, D. Badikov, and V. Petrov, "Difference-frequency generation of ultrashort pulses in the mid-IR using Yb-fiber pump systems and AgGaSe 2." *Opt. Express* **23**, 2730 (2015).
27. M. Knorr, J. Raab, M. Tauer, P. Merkl, D. Peller, E. Wittmann, E. Riedle, C. Lange, and R. Huber, "Phase-locked multi-terahertz electric fields exceeding 13 MV/cm at a 190 kHz repetition rate," *Opt. Lett.* **42**, 4367 (2017).
28. C. Gaida, M. Gebhardt, T. Heuermann, F. Stutzki, C. Jauregui, J. Antonio-Lopez, A. Schülzgen, R. Amezcua-Correa, A. Tünnermann, I. Pupeza, and J. Limpert, "Watt-scale super-octave mid-infrared intrapulse difference frequency generation," *Light Sci. Appl.* **7**, 94 (2018).
29. J. Zhang, K. F. Mak, N. Nagl, M. Seidel, D. Bauer, D. Sutter, V. Pervak, F. Krausz, and O. Pronin, "Multi-mW, few-cycle mid-infrared continuum spanning from 500 to 2250 cm^{-1} ," *Light Sci. Appl.* **7**, 17180 (2018).
30. M. J. Weber. *Handbook of optical materials*. CRC press, 2002.
31. D. Sánchez, M. Hemmer, M. Baudisch, K. Zawilski, P. Schunemann, H. Hoogland, R. Holzwarth, and J. Biegert, "Broadband mid-IR frequency comb with CdSiP 2 and AgGaS 2 from an Er, Tm: Ho fiber laser," *Opt. Lett.* **39**, 6883 (2014).
32. T. Lang, A. Harth, J. Matyschok, T. Binhammer, M. Schultze, and U. Morgner, "Impact of temporal, spatial and cascaded effects on the pulse formation in ultra-broadband parametric amplifiers," *Opt. Express* **21**, 949 (2013).
33. K. L. Vodopyanov, "Optical THz-wave generation with periodically-inverted GaAs," *Laser Photonics Rev.* **2**, 11 (2008).
34. Z.-S. Feng, Z.-H. Kang, F.-G. Wu, J.-Y. Gao, Y. Jiang, H.-Z. Zhang, Y. M. Andreev, G. V. Lanski, V. V. Atuchin, and T. A. Gavrilova, "SHG in doped GaSe: In crystals," *Opt. Express* **16**, 9978 (2008).
35. A. Baltuška, T. Fuji, and T. Kobayashi, "Controlling the Carrier-Envelope Phase of Ultrashort Light Pulses with Optical Parametric Amplifiers," *Phys. Rev. Lett.* **88**, 133901 (2002).
36. G. Cerullo, A. Baltuška, O. Mücke, and C. Vozzi, "Few-optical-cycle light pulses with passive carrier-envelope phase stabilization," *Laser Photonics Rev.* **5**, 323 (2011).
37. L. von Grafenstein, M. Bock, D. Ueberschaer, U. Griebner, and T. Elsaesser, "Ho:YLF chirped pulse amplification at kilohertz repetition rates—4.3 ps pulses at 2 μm with GW peak power," *Opt. Lett.* **41**, 4668 (2016).